Mon. Not. R. Astron. Soc. **000**, 000–000 (0000) Printed 13 April 2016 (MN LATEX style file v2.2)

Ionisation and discharge in cloud-forming atmospheres of brown dwarfs and extrasolar planets

Ch. Helling[1⋆], P. B. Rimmer[1], I. M. Rodriguez-Barrera[1], Kenneth Wood[1], G.B. Robertson[1], C.R. Stark[2]
[1] *SUPA, School of Physics and Astronomy, University of St Andrews, St Andrews KY16 9SS, UK*
[2] *Division of Computing and Mathematics, School of Arts, Media and Computer Games, Abertay University, Dundee DD1 1HG, UK.*

13 April 2016

ABSTRACT
Brown dwarfs and giant gas extrasolar planets have cold atmospheres with a rich chemical compositions from which mineral cloud particles form. Their properties, like particle sizes and material composition, vary with height, and the mineral cloud particles are charged due to triboelectric processes in such dynamic atmospheres. The dynamics of the atmospheric gas is driven by the irradiating host star and/or by the rotation of the objects that changes during its lifetime. Thermal gas ionisation in these ultra-cool but dense atmospheres allows electrostatic interactions and magnetic coupling of a substantial atmosphere volume. Combined with a strong magnetic field $\gg B_{\rm Earth}$, a chromosphere and aurorae might form as suggested by radio and X-ray observations of brown dwarfs. Non-equilibrium processes like cosmic ray ionisation and discharge processes in clouds will increase the local pool of free electrons in the gas. Cosmic rays and lighting discharges also alter the composition of the local atmospheric gas such that tracer molecules might be identified. Cosmic rays affect the atmosphere through air showers in a certain volume which was modelled with a 3D Monte Carlo radiative transfer code to be able to visualise their spacial extent. Given a certain degree of thermal ionisation of the atmospheric gas, we suggest that electron attachment to charge mineral cloud particles is too inefficient to cause an electrostatic disruption of the cloud particles. Cloud particles will therefore not be destroyed by Coulomb explosion for the local temperature in the collisional dominated brown dwarf and giant gas planet atmospheres. However, the cloud particles are destroyed electrostatically in regions with strong gas ionisation. The potential size of such cloud holes would, however, be too small and might occur too far inside the cloud to mimic the effect of, e.g., magnetic field induced star spots.

1 INTRODUCTION

The presence of atmospheric clouds outside the solar system has now been established through multi-wavelength variability observations for brown dwarfs and through transit spectroscopy in extrasolar planets as summarized in Helling & Casewell (2014) and Marley et al. (2013). Theoretical efforts have focused on modelling the thermodynamic and chemical structure of such ultra-cool atmosphere in order to predict their spectral appearance from the optical into the far-infrared spectral region (Allard 1995; Burrows et al. 1997; Marley et al. 2002; Fortney et al. 2008; Witte et al. 2011). A keystone in this efforts is the modelling of cloud formation and cloud feedback on the atmosphere. Clouds impose an opacity that is considerably larger than that of the gas (main gas opacity sources: CO/CH_4, H_2O, TiO/VO, Na, K), and they deplete or enrich the element abundance inhomogeneously (e.g. Fe, Mg, Si, O, Ti, Al).

Recently, observations in the near infrared (Sorahana, Suzuki & Yamamura 2014) and in Hα indicate potential chromospheric emission (Schmidt et al. 2015) which would suggest a outward temperature increase in the atmosphere of brown dwarf. Previously, brown dwarf atmospheres were considered too cold to exhibit any characteristic plasma signature (Mohanty et al. 2002). Radio observations of brown dwarfs support the expectation that the atmospheres of brown dwarfs exhibit plasma behaviour (e.g. Hallinan et al. 2015), and open up the possibility to study the magnetic behaviour of such ultra-cool objects. Interpretations of such radio detection at present invoke the electron cyclotron maser instability as reason for radio emission at 1 - 100GHz which requires a large magnetic field strength at the site where the cyclotron maser criterion is fulfilled (Vorgul et al. 2011). As the cyclotron frequency, ν_c, scales with the local magnetic field strength B as $\nu_c = eB/(2\pi m_e\, c)$, a magnetic field strength of $>$ 34kG is required, for example, in the case of the M9.5 brown dwarf TVLM 51346546 which was observed to emit at $\sim$ 100GHz (Williams et al. 2015) for cyclotron emission to occur. Typical magnetic field strength for such late M-dwarfs/brown dwarfs are $O(10^3)$G which

is 30× lower than required for cyclotron emission. A more suitable interpretation seems that the TVLM 513 emission detected by ALAMA originates from a population of near speed-of-light (weakly relativistic) electrons in the form of gyrosynchrotron emission, maybe comparable to Auroral km emission on Uranus. Aurora observations from the solar system start to emerge as guide for radio emission on brown dwarfs (Nichols et al. 2012; Hallinan et al. 2015). All mechanisms, the cyclotron maser instability and Auroral emission, however, require a pool of free electrons that are captured by the magnetic field and therefore can emit as accelerated charges. The challenge is that no brown dwarf has been found to orbit a Sun-like host star from which it could pick up charges from the stellar wind like the solar system planets nor can we assume without proof that brown dwarfs host geologically active moons to provide a steady stream of charges like in the case of the Jupiter moon Io. Studies of possible ionisation processes occurring in the ultra-cool atmospheres of brown dwarfs are therefore conducted, and Section 2 discusses processes that effect the ionisation state of ultra-cool atmospheres. Main results of a recent reference study will be summarised against which the effect of additional processes, like Cosmic Ray ionisation or lightning discharges in clouds, can be compared for understanding the radio emission from ultra-cool atmospheres. The DRIFT-PHOENIX atmosphere models utilised here as input for the local gas temperature, gas pressure, thermal electron number density and cloud properties are 1D atmopshere simulations (Helling et al. 2008a,b; Witte, Helling & Hauschildt 2009; Witte et al. 2011). We therefore performed 3D Monte Carlo radiative transfer simulations of Cosmic Ray induced air showers to understand how spatially extended the effect of Cosmic Rays on the local atmospher might be and how this may differ from our previous 1D results. Section 3 investigates the charging of mineral cloud particles through thermal collisions with the atmospheric gas to provide a first insight into the possible number of charges that a mineral cloud particle can carry in comparison to their stability against charge induced destruction processes. We argue that regions with strong local gas ionisation, like Alfvén ionisation, would lead to the destruction of the cloud particles in this regions which could then mimic the appearance of cold spots on the brown dwarf's surface. Electrostatic cloud destruction would also help to understand the increasing variability across the spectral L-T transition for brown dwarfs (e.g. Gizis et al. 2015). However, our scale estimates show that the resulting cloud holes are too small and potentially too deep inside the cloud to have an observational effect.

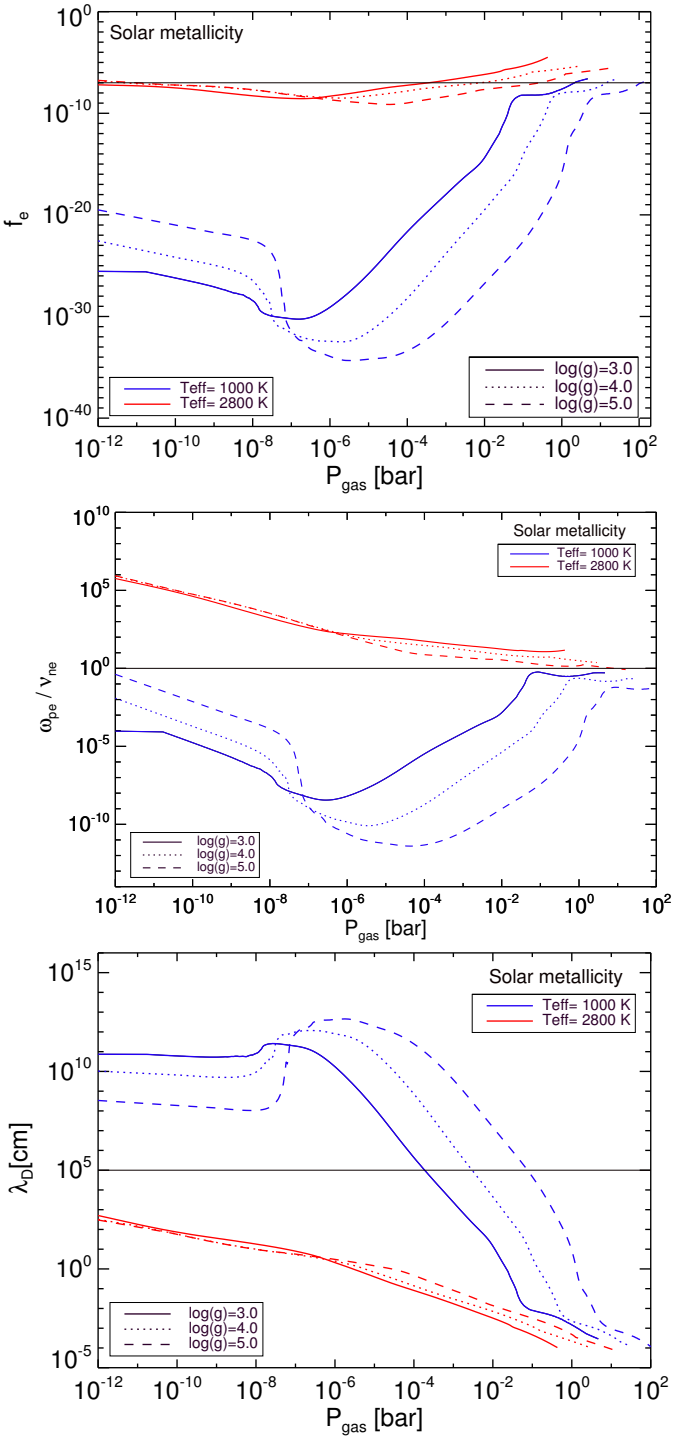

Figure 1. Characterising the thermal ionisation state in ultra-cool atmosphere: **Top:** local degree of thermal ionisation f_e, **Middle:** plasma frequency vs. kinetic collisional frequency between electrons and neutrals, ω_{pe}/ν_{ne} ($\nu_{ne} = \sigma_{gas} n_{gas} v_{th,e}$, σ_{gas} – scattering cross section, $v_{th,e} = \sqrt{k_B T_e / m_e}$ – thermal velocity of electrons, k_B – Boltzmann constant)

2 SOURCES OF FREE ELECTRONS IN ULTRA-COOL ATMOSPHERES

2.1 Thermal ionisation

Thermal ionisation provides the background ionisation in every atmospheric gas according to the local gas temperature and pressure. A reference study of the ionisation and magnetic coupling behaviour for the atmospheres of ultra-cool objects considering thermally ionisation can be conducted on the base of existing model atmosphere grids. We utilise a grid of DRIFT-PHOENIX model atmosphere simulations

which include cloud formation modelling. The grid models cloud forming atmospheres of M dwarfs, brown dwarfs and giant gas planets. Rodríguez-Barrera et al. (2015) use the whole set of models, here we only apply a subset. Each atmosphere model is determined by global parameters that unambiguously characterise a specific object. The global parameter for a giant gas planet atmosphere model would be the total flux $T_{\rm eff}$ =1000K, the surface gravity log(g)=3.0; for a brown dwarf it would be $T_{\rm eff}$ =1000K, the surface gravity log(g)=5.0, plus a set of element abundances. A M dwarf (or a young brown dwarf) would have a higher effective temperature, $T_{\rm eff}$ = 2800K, and a lower surface gravity of log(g)=4.0([1]). The (initial) element abundances are assumed to be solar but they are altered by element depletion or enrichment because of cloud formation or evaporation. DRIFT-PHOENIX solves equations for non-equilibrium kinetic cloud formation (Woitke & Helling 2003; Helling & Woitke 2006; Helling, Woitke & Thi 2008a; Helling & Fomins 2013), hydrostatic and chemical equilibrium, and uses mixing length theory and radiative transfer theory to calculate the temperature structure (Hauschildt & Baron 1999). DRIFT-PHONENIX describes the formation of cloud particles as a phase transition process by considering seed formation, grain growth and evaporation, sedimentation, element depletion and the feedback of these processes on the atmosphere structure (Woitke & Helling 2004; Helling et al. 2008a,b; Witte, Helling & Hauschildt 2009; Witte et al. 2011). The resulting 1D atmosphere structures are characterised by their local gas temperature, $T_{\rm gas}$ [K], and gas pressure, $p_{\rm gas}$ [bar], but also by a cloud structure with results for material composition of the cloud particles, cloud particle size, cloud particle and gas-phase number densities, all depending on height. These values allow to derive the local degree of ionisation $f_{\rm e}(z) = n_{\rm e}(z)/n_{\rm gas}(z)$ ($n_{\rm gas}(z) = p_{\rm gas}(z)/(k_{\rm B}T_{\rm gas}(z))$ – total gas number density [cm^{-3}], $k_{\rm B}$ – Boltzmann constant, $n_{\rm e}(z)$ – electron number density [cm^{-3}]), the plasma frequency, $\omega_{\rm pe} = \sqrt{n_{\rm e}e/(\epsilon_0 m_{\rm e})}$ (e – electron charge [C], $m_{\rm e}$ – electron mass), and the Debye length $\lambda_{\rm D} = \sqrt{\epsilon_0 k_{\rm B}T_{\rm e}/(n_{\rm e}e^2)}$. A certain ionisation is required for a plasma to establish long-distance electrostatic interactions. Figure 1 (top) demonstrates that the local degree of thermal ionisation is rather low throughout the low-temperature atmospheres depicted. It, however, reaches a certain threshold of $f_{\rm e} > 10^{-7}$ (horizontal line) in the inner (high pressure) atmosphere above which experiments suggest plasma behaviour to set in. The comparison between the plasma frequency, $\omega_{\rm pe}$, and the electron-neutral collision frequency, $\nu_{\rm ne}$, demonstrate that the upper, low pressure part of the atmosphere is most susceptible to long-range electrostatic interactions, i.e. where $\omega_{\rm pe}/\nu_{\rm ne} \gg 1$. The Debye length shows over which length scale such electrostatic interactions can be expected to occur and Fig. 1 (bottom) shows that they are particularly large for the atmospheres with the lowest effective temperature $T_{\rm eff}$, in the upper atmosphere where the degree of ionisation is smallest.

For a charged particle's motion to be dictated by a magnetic field, and hence producing radio emission, the particle needs to complete a considerable number of gyrations before a collision with a neutral atom occurs. If this charged particle is, for example, an electron, the comparison between the electron cyclotron frequency, $\omega_{\rm c,e} = eB/m_{\rm e}$ and the electron-neutral collision frequency, $\nu_{\rm n,e}$ allows to derive a critical value for the local magnetic field for a magnetic coupling of the gyrating ionised species. The critical local magnetic field for electrons to be magnetically bound is $B_{\rm e} \gg (m_{\rm e}/e)\sigma_{\rm gas}n_{\rm gas}\sqrt{k_{\rm B}T_{\rm e}/m_{\rm e}}$ which is independent on the local state of gas ionisation (for more details see Rodríguez-Barrera et al. 2015). Figure 2 shows that the upper parts of ultra-cool atmospheres are magnetically coupled for both, electrons and atomic ions, in brown dwarfs and giant gas planets. A comparison to the magnetic field densities expected for M dwarfs, brown dwarfs and giant gas planets (horizontal lines) shows that a larger atmospheric volume can be magnetically coupled in a brown dwarf atmosphere than in a giant gas planet atmosphere.

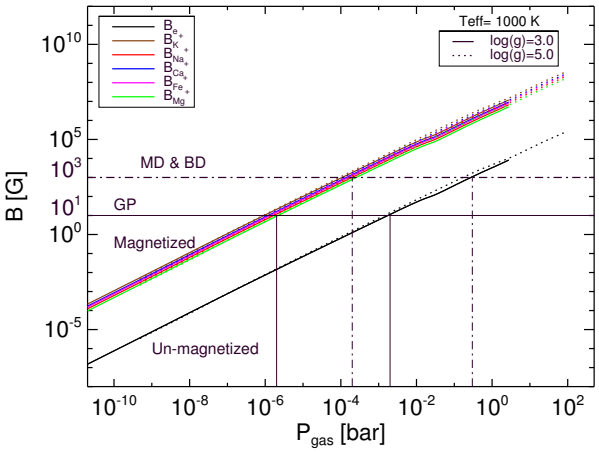

Figure 2. The magnetic coupling of ultra-cool and thermally ionisaed atmospheres. Horizontal lines indicate typical magnetic field densities for M dwarfs and Brown Dwarfs (10^3G), and giant gas planets (10 G). Vertical lines link these values with the gas pressure where these field strength would occur inside the atmosphere. The equivalent global Earth magnetic field strengths is ≈ 0.3 G.

2.2 Non-thermal processes: winds, clouds and cosmic rays

Brown dwarfs are fast rotators which causes the atmosphere to develop winds. Giant gas planets develop strong winds due to the strong irradiation by their host stars. Global circulation models for giant gas planets (Showman et al. 2008; Dobbs-Dixon, Cumming & Lin 2010; Dobbs-Dixon & Agol 2013; Showman, Lewis & Fortney 2015) suggest local wind speeds of several km s^{-1}. High wind speeds are reached in the equatorial jet streams in the upper atmosphere of the giant gas planet HD 189 733b, for example. Zhang & Showman (2014) demonstrate, however, that the global wind speed does not exceed 0.2-0.5 km s^{-1} in brown dwarf atmospheres based on their present set of 3D atmosphere simulations. Diver, Fletcher & Potts (2005) demon-

[1] see https://leap2010blog.wordpress.com/category/drift-phoenix/ for a summary of DRIFT-PHOENIX atmosphere modelling

strate that a wind speed of $2-5$ km s^{-1} is required to allow the collisions of the wind with the ions to cause a charge imbalance resulting in a considerable increase of the local degree of ionisation. The required magnetised seed plasma will keep the electrons locked in place by a magnetic field to allow the wind to push away the ions which have a considerably larger collisional cross section than electrons. Therefore, the local charge imbalance imposed by the gas flow must be established on a timescale, $\tau_{\rm s} = m_{\rm i}/(q_{\rm i}B)$ ($\omega_{\rm i} = q_{\rm i}B/m_{\rm i}$ – ion cyclotron frequency, $q_{\rm i}$ – ion charge, $m_{\rm i}$ – ion mass), shorter than that for electron transport to neutralise it again. Stark et al. (2013) apply this idea to brown dwarf atmospheres. However, this time scale might be more appropriately represented by the collisional frequency with the neutral gas as brown dwarf/ giant gas planet atmospheres have very high densities, $\tau_{\rm s} \sim \nu_{\rm ni}$ with $\nu_{\rm ni} \approx \pi r_{\rm H_2}^2 \times n_{\rm gas} v_{\rm th,i}$, $v_{\rm th,i} = (k_{\rm B}T_{\rm i}/m_{\rm i})^{-1/2}$, and $T_{\rm i} = T_{\rm gas}$. Assuming that the ions follow the wind, the size of the pocket of such an Alfvén ionised gas can be estimated from $R_{\rm Alf} \approx v_{\rm wind}/\nu_{\rm ni}$.

Figure 2 shows that in particular the upper, low-pressure regions of an atmosphere can be expected to be magnetically coupled. Alfvén ionisation will therefore work best at gas pressures $<$ 1bar in brown dwarf atmospheres and $< 10^{-2.5}$bar in giant gas planet atmospheres. This pressure range coincides with the atmospheric range where mineral clouds form in brown dwarfs and giant gas planets (Fig. 2 in Helling, Woitke & Thi 2008b). This suggests that the charge imbalance caused by the impact of strong winds on a magnetised plasma could contributes to cloud particle ionisation in these pockets of Alfvén ionisation.

Helling, Jardine & Mokler (2011) argue that clouds in brown dwarf and giant gas planet atmosphere are electrostatically charged because particle-particle collisions in turbulent atmosphere clouds alone are energetic enough to overcome the work function of mineral materials (triboelectric charging). The size-dependent gravitational settling (rain-out), which determines the cloud height, causes a large scale charge separation resulting in an electrostatic potential difference inside such a mineral cloud. Helling et al. (2013) demonstrated that such a potential difference can overcome the breakdown field and, hence, initiate an ionisation avalanche that subsequently can lead to a large-scale lighting discharge inside mineral clouds. Bailey et al. (2014) use scaling laws derived from sprite experiments and demonstrate that such large-scale discharges can reach an geometrical extension of $\approx$ 3000km in brown dwarf clouds but only $\approx$ 300km in a giant gas planet atmosphere.

Cosmic rays (CR) contribute to the ionisation of clouds on Earth and they are discussed as trigger for lighting initiation in the Earth atmosphere (Gurevich & Karashtin 2013). Similar effects occur in brown dwarfs and extrasolar planets (Rimmer & Helling 2013) where each of the systems may be exposed to a different radiation field of a host star or the interstellar medium irradiated by a high-mass O- or B-type star. For the interstellar cosmic ray flux spectrum (e.g., Fig. 4 in Rimmer & Helling 2013), the local degree of gas ionisation increases by $\approx$ 6 orders of magnitude in the case of a giant gas planet atmosphere and by $\approx$ 4 orders in a brown dwarf atmosphere that is $10^2\times$ more compact. Cosmic rays do also effect the abundance of molecules through ion-neutral kinetic gas chemistry by opening up reaction channels to more and more complex hydro-carbon molecules (Rimmer, Helling & Bilger 2014). The investigation of the spatial extent of CR triggered events is required to help determining how much of the atmosphere volume might produce chemical tracers. So far, only 1D simulations were done for extrasolar objects (Rimmer & Helling 2013).

We therefore carried out first 3D radiative transfer calculations utilizing the Monte Carlo method (Wood & Reynolds 1999) which has been updated to include algorithms for particle tracking from Dupree & Fraley (2002) as a follow-up of the work presented in Rimmer & Helling (2013) for hydrogen-rich atmospheres. We model the interactions of protons, positive, neutral and negative pions, positive and negative muons, electrons and positrons, and gamma rays with an H_2-dominated gas in a three dimensional Cartesian grid representing a homogeneous atmosphere with a radial density-temperature gradient. The atmosphere profile that determins the density-temperature gardient is the same like in Rimmer & Helling (2013) (their Fig. 3) and is used as input for the local gas number density. The 3D atmosphere is assumed to be isotropic, the density profile only changing with the distance from the center as prescribed by the 1D profile. The air shower is initiated by one CR event which is assumed to have an energy of 10^{20}eV. Rimmer & Helling (2013) demonstrated that high-energy CR events penerate deeper into the atmosphere. This approach therefore allows us to study the maximum effect on the atmospheric volume influenced by one air shower event. Rimmer & Helling (2013) have studied the CR electron production rate for a whole spectrum of intial CR energies but in 1D. Here, we are interested in the geometrical extent of such an event skimming the atmosphere for allowing a maximum of observable volume. For an air shower intiated by one CR event, the number of particles exceeds a million within just a few generations after initiation. We apply a thin sampling method where all particles below a predefiened thinning energy level are subject to thin sampling with a chance of survival proportional to their energy (Hillas 1985; Hillas 1997). The shower development can then be studied, for example, by measuring the penetrative depth of an air shower, called shower age s, which depends in the integrated column density (see Eq. 3 in Rimmer, Stark & Helling 2014). The shower age is, for example, used to parameterise the energy distribution of secondary electrons (see Eq. 4 in Rimmer, Stark & Helling 2014). The shower age can only be determined in one direction, and Figure 4 shows the shower age for the radial direction. The air shower reaches its maximum at a radial depth of r=1.0013 $R_{\rm Jupiter}$ for a Jupiter-like atmosphere. This value is expected to be lower for denser atmospheres like for brown dwarfs, hence the impact of CRs on the electron gas density will be smaller in Brown Dwarfs than in Jupiter-like planets.

Figure 3 shows results in 2D cuts for an air shower triggered by an CR event of 10^{20}eV. Note that the longitudinal extension of the shower is approximately two orders of magnitude greater than the lateral extension. The opening angle of the air shower remains rather confined despite various singular trajectories branching out. The shower has no significant anisotropies in the x-y plane (Fig. 3, right). Images of the other particle types appear vastly different, for example, the trajectories of neutral pions are mostly sub-centimetre because they decay almost instantaneously, hence, only effect the uppermost atmosphere.

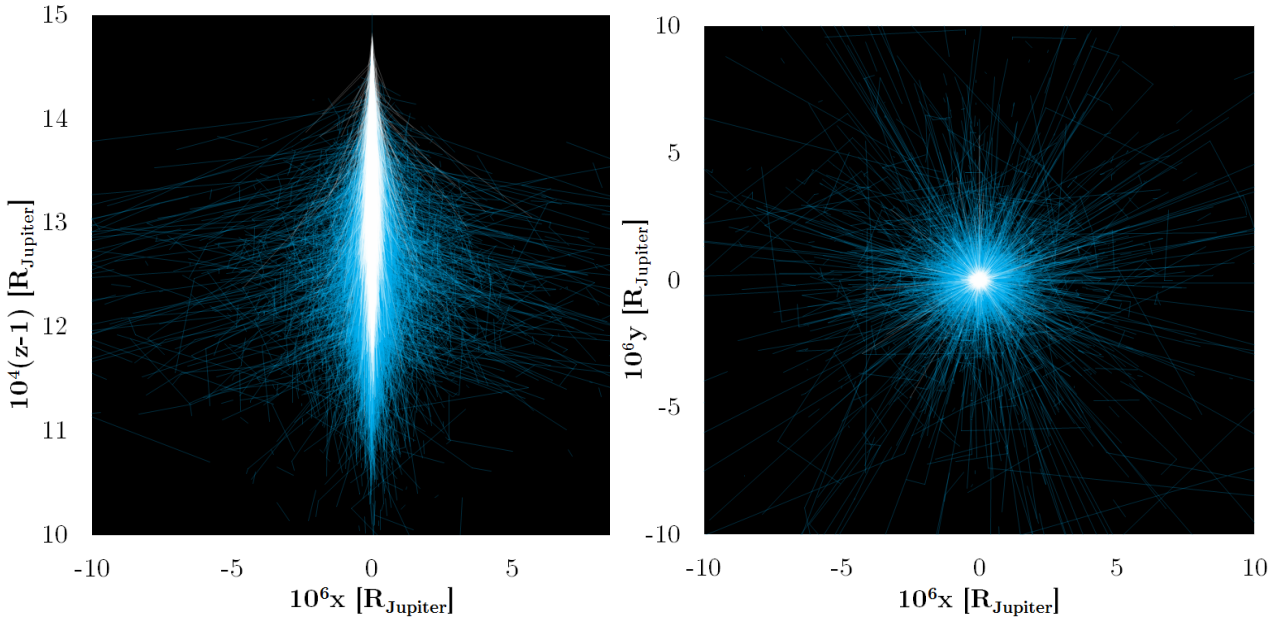

Figure 3. 3D Monte Carlo simulation of a Cosmic Ray triggered air shower in a Jupiter-like atmosphere. The proton trajectoriers (blue) and the positive pions (white) are triggered by a primary CR event of 10^{20}eV. **Left:** z-y plane view, **Right:** view in direction of motion with the CR at an zero angle into the atmosphere (x-y plane). The figure demonstrates that the air shower remains rather confined with respect of the atmospheric volume effected. The use of 1D simulation to calculate the CR spectrum impact on the electron budget appear therefore suitable.

Our 3D results confirm that also in extrasolar objects only the uppermost atmospheric layers will be affected by cosmic air showers because of the rather high local densities in the atmospheres of giant gas planets and brown dwarfs. Their occurrence statistics will depend on the external cosmic ray flux which will be higher for young brown dwarfs in a star forming regions with strongly radiating O- and B-stars or for an object near a super nova outburst compared to an extrasolar planet in a planetary system around a Sun-like star.

3 CHARGING CLOUD PARTICLES BY ATMOSPHERIC GAS INTERACTION

Atmospheres of extrasolar planets have been shown to form clouds that are made of mixed mineral particles of various sizes (e.g., Helling, Woitke & Thi 2008b). The growth of these cloud particles is determined by collisions with the ambient gas which they deplete. Cloud particles start to gravitational settle and change their size and composition depending on the local thermodynamic conditions. The distance over which the cloud particle ensemble precipitates does determine the geometrical height of the cloud. Cloud particle will not only collide with neutral species, but also with electrons and ions and by this process pick up charges from the surrounding atmospheric gas. The efficiency of this charging process will depend on the abundance of the electrons and ions in the gas phase and their temperature. In extrasolar, ultra-cool atmosphere, the amount of free charges will be moderate as discussed in Sect. 2.1 if thermal ionisation is the only gas ionisation process. Section 2.2 summarised other processes that act to increase the pool of free charges in ultra-cool atmospheres. A background of thermal electrons will therefore always be present. In following section, we offer a first exploration of how such atmospheric charges may effect the cloud particle charges, and argue that regions of strong gas ionisation destroy cloud particles electrostatically. If such a destruction occurs, the cloud opacity would change and possibly allow for an observable change of radiation flux.

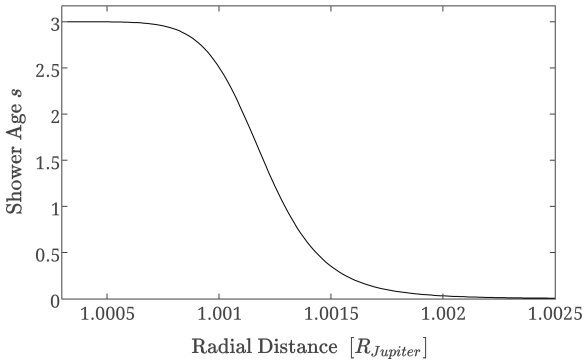

Figure 4. The air shower penetration depth (shower age), $s = s(X)$ (X - column density) for a Jupiter-like atmosphere and a CR event of 10^{20}eV: $s = 0$ corresponds to the initial event, $s = 1$ corresponds to the shower maximum occuring at r=1.0013 $R_{Jupiter}$, and $s = 3$ for in infinit column density $X \to \infty$.

3.1 Electron Deposition on cloud particles in ultra-cool atmospheres

We perform a first exploratory estimate of atmospheric regions of extrasolar planets and brown dwarfs where cloud

particles are most likely to be stable against electrostatic disruption caused by charges accumulation on their surfaces. As a first attempt to evaluate cloud particle charging in brown dwarf atmospheres, electron deposition on cloud particle is considered as a first order process where the respective rate coefficient depends only linearly on the gas density, $k \sim n_{\rm gas}$. Gas-phase ionisation mechanisms were discussed in Sect 2 for brown dwarfs and extrasolar planetary atmospheres. The cloud particles are assumed to be spherical. The gas-phase ionisation is parameterised by an ionisation rate ζ [s^{-1}]. Electrons are adsorbed onto the surface of a cloud particle with a certain probability when the electron in the atmospheric gas collides with the cloud particle. Similar to the growth of cloud particles by gas-surface reactions (Woitke & Helling 2003), the electron will approach the surface directly (free molecular flow) or diffusive (viscous) before the electrostatic interaction dominates. We assume that electrostatic attraction/repulsion will dominate the approach of the electron or ion. Considerably more elaborate approaches have been published for dust charging in protoplanetary disks by e.g. Fujii, Okuzumi & Inutsuka (2011); Ilgner (2012). We aim to provide this first estimate in combination with our detailed modelling of cloud formation which provides the local cloud particle number density, $n_{\rm d}$ [cm^{-3}], their size, a [cm], and material composition which is a mix of materials (Woitke & Helling 2004; Helling & Woitke 2006; Helling, Woitke & Thi 2008a), in contrast to previous works. Mineral clouds in brown dwarfs and giant gas planets are characterised by cloud particles changing in size and material composition depending in the local temperature and gas density. Gnerally, the top of the cloud is dominated by small particles (10^{-6}cm) and a mix of Mg/Si/Fe/O materials (see Tabe 7 in Helling, Woitke & Thi 2008b). The cloud base can be made of particles a large as 10^{-2}cm which predominently contain high-temperature condensates made of Fe/Al/Ti/O. These findings are based on a kinetic cloud formation models that described seed formation and subsequent surface growth/evaporation by gas phase - surface reactions. The model derived by Woitke & Helling (2004); Helling & Woitke (2006); Helling, Woitke & Thi (2008a) does fulfil element conservation and takes into account gravitational settling and convective mixing for the cloud particle formation.

In the following, a locally constant grain size is assumed. Changes in grain size could inprinciple occur but are not considered in our following explorative estimate.

The net number of electrons per grain (net negative charge), $N_{\rm e,d}$, changes depending on the local electron number density, n_e, through electron and ion adsorption as

$$\frac{dN_{\rm e,d}}{dt} = (k_- - k_+) n_e. \quad (1)$$

The electron number density, $n_{\rm e}$, in the gas phase changes therefore through cloud particle ionisation as

$$\frac{dn_e}{dt} = \zeta n_{\rm gas} - \alpha n_e^2 - k_- n_{\rm d} n_e. \quad (2)$$

The first term parameterises the gas ionisation by a prescribed ionisation rate ζ [s^{-1}]. The second term describes the gas-phase recombination the third term is the loss through the adsorption of an electron onto the grain surface. The total rate coefficient for recombination in the gas-phase, α [cm^3 s^{-1}], can be written as

$$\alpha = \alpha_2 + n_{\rm gas}\alpha_3, \quad (3)$$

where α_2 [cm^3 s^{-1}] is the 2-body gas-phase recombination rate, and α_3 [cm^6 s^{-1}] is the 3-body rate:

$$\alpha_2 = 8.22\times10^{-8}\left(\frac{T}{300{\rm K}}\right)^{-0.48} - 1.3\times10^{-8}, \quad (4)$$

$$\alpha_3 = 2\times10^{-25}\left(\frac{T}{300{\rm K}}\right)^{-2.5}. \quad (5)$$

The adsorption rate for electrons onto a cloud particle, k_-, and for ions k_+, both with units [cm^3 s^{-1}], can be expressed as

$$k_- = \sigma_{\rm gr}\sqrt{v_e^2 - \frac{N_{\rm e,d}e^2}{2\pi\epsilon_0 m_e a}}, \quad (6)$$

$$k_+ = \sigma_{\rm gr}\sqrt{\frac{8k_{\rm B}T}{\pi m_p} + \frac{N_{\rm e,d}e^2}{2\pi\epsilon_0 m_p a}}, \quad (7)$$

where $k_{\rm B} = 1.38\times10^{-16}$ erg/K is Boltzmann's constant, v_e [cm/s] is the electron velocity, $m_e = 9.11\times10^{-28}$ g, and $m_p = 1.67\times10^{-24}$ g. The cross-section for a spherical dust grain is $\sigma_{\rm gr} = \pi a^2$, with e the elementary charge and ϵ_0 the permittivity of free space. The second terms in Eqs. 6, 7 account for the effect of the electrostatic field of the negatively charged grain upon the gas-phase electrons and ions. The free electrons are not necessarily in thermal equilibrium with the ambient neutral gas, or the ions. Brown dwarf atmospheres are, however, very dense and therefore collisional dominated. We use $T_{\rm e} = T_{\rm i} = T_{\rm gas}$ unless stated otherwise. The velocity of the electron is therefore taken to be its thermal velocity, $v_{\rm e} = v_{\rm th,e}$. This will, however, not be true during the development of a discharge or other high-energy events. As the number of surface electrons grows, the resulting electrostatic field of the cloud particle begins to inhibit further electron attachment. However, the field attracts ions and now the probability of ion attachment increases. Ion attachment neutralises the grain, lowering the net negative charge of the grain.

The steady-state solution of Eq. (1), $dN_{\rm e,d}/dt = 0$, is satisfied when $k_- = k_+$ (Eqs. 6, 7). The maximum value, $N_{\rm e,d,max}$, of charges that a cloud particle of size a can acquire by adsorption from a surrounding ionised gas of temperature $T = T_{\rm gas}$ is therefore

$$N_{\rm e,d,max} = \Big(\frac{16k_B\epsilon_0}{e^2}\Big)aT. \quad (8)$$

The quantity $N_{\rm e,d,max}$ denotes the number of electrons a grain will have at steady state. $N_{\rm e,d,max}$ is independent of the gas ionisation rate ζ (Eq. 2). Processes that requires a critical surface charge, $N_{\rm d,crit}$, will occur if $N_{\rm d,crit} < N_{\rm e,d,max}$ (e.g. electrostatic disruption, Stark, Helling & Diver 2015; electron avalanches, Helling et al. 2011; Dubrovin et al. 2015). If $N_{\rm d,crit} > N_{\rm e,d,max}$, than the number of electrons on the cloud particle surface would achieve steady state before the critical process has a chance to occur. The time needed to achieve steady state is characterised by $k_- \neq k_+$, and hence $N_{\rm e,d} \ll N_{\rm e,d,max}$. In this case, the electrostatic contributions to the adsorption rates k_- and k_+ become very

small, and Eqs. 6 and 7 can be approximated by

$$k_- = \sigma_{\rm gr} v_e, \tag{9}$$

$$k_+ = \sigma_{\rm gr} \sqrt{\frac{8kT}{\pi m_p}}. \tag{10}$$

3.2 Time evolution of cloud particle changing

Equation 2 can be integrated to obtain an analytic expression for the gas electron number density, n_e, that changes because of electron depletion through grain collisions before steady state is reached or if it is not reached at all

$$n_e = \frac{1}{\alpha\tau} \tanh\left[\frac{t}{\tau} + \operatorname{arctanh}\left(\frac{k_- n_{\rm d}\tau}{2}\right)\right] - \frac{k_- n_{\rm d}}{2\alpha}, \tag{11}$$

with

$$\tau = \frac{2}{\sqrt{4\alpha\zeta n_{\rm gas} + k_-^2 n_{\rm d}^2}}. \tag{12}$$

The first term in Eq. 12 represent the electron-gas recombination, the second term the electron adsorption onto the grain's surface. Inserting Eq. 11 into Eq. 1 results in

$$\frac{dN_{\rm e,d}}{dt} = \frac{k_- - k_+}{\alpha\tau} \tanh\left[\frac{t}{\tau} + \operatorname{arctanh}\left(\frac{k_- n_{\rm d}\tau}{2}\right)\right] - \frac{(k_- - k_+)k_- n_{\rm d}}{2\alpha}. \tag{13}$$

Integrating Eq. (13) results in an expression for the total number of charges, $N_{\rm e,d}$, on an ensemble of cloud particles due to a first-order gas-phase ionization process as a function of time before steady state is achieved,

$$N_{\rm e,d} = \frac{k_- - k_+}{\alpha} \log\left[\cosh\left(\frac{t}{\tau} + \operatorname{arctanh}\left(\frac{k_- n_{\rm d}\tau}{2}\right)\right)\right] - \frac{(k_- - k_+)k_- n_{\rm d} t}{2\alpha} - \frac{k_- - k_+}{\alpha} \log\left[\left(1 - \frac{k_-^2 n_{\rm d}^2 \tau^2}{4}\right)^{-1/2}\right]. \tag{14}$$

This solution is only accurate when $N_{\rm e,d} \ll N_{\rm e,d,max}$, hence before the cloud particles have achieved a charge steady state. The predicted time (Eq. 12) can only be considered as a lower limit because the electrostatic effects of the charged grain on free electrons and cations is neglected in our approximations of Eq's. (9) and (10) which have not been used in the whole of Sect. 3.2.

For spherical grains the maximum number of net charges that can reside on a grain of radius a before Coulomb explosion can be expressed as (Eq. 8 in Stark, Helling & Diver 2015),

$$N_{\rm ce} = \frac{\pi(32\epsilon_0\Sigma_s)^{1/2}}{e} a^2, \tag{15}$$

with Σ_s he mechanical tensile strength of the dust grain (the maximum stress or pressure that a material material can withstand). By setting $N_{\rm e,d} = N_{\rm ce}$ (Eqs. 14 and 15), a critical time scale, $t_{\rm crit}$, can than be evaluated numerically. $t_{\rm crit}$ is the time during which the cloud particle can accumulate charges by electron deposition and still be stable agains

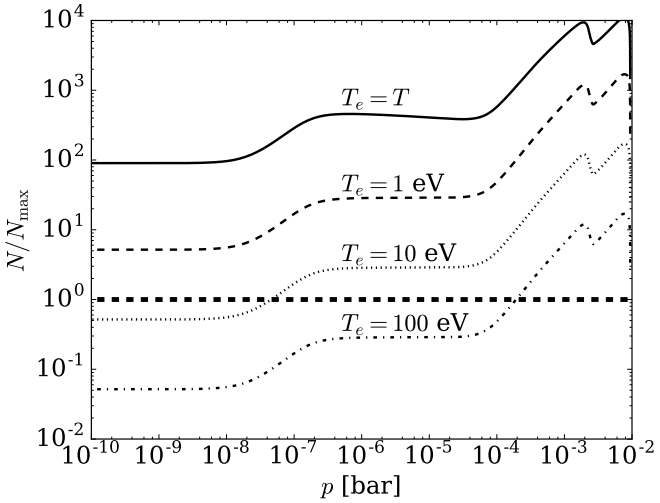

Figure 5. The electron number ratio $N/N_{\rm max}$ (Eq. 16) for a mineral cloud formed in a giant gas planet or brown dwarf with $T_{\rm eff}$ = 1600K, $\log g$ = 3 and solar element abundance. Different electron temperatures, $T_e = T_{\rm gas}$ ($\approx$ 0.1eV), 1 eV ($\approx 10^4$K), 10 eV ($\approx 10^5$K) and 100 eV ($\approx 10^6$K), are evaluated. The horizontal lines represents $N_{\rm ce}/N_{\rm max} = 1$. The cloud particles are stable against electrostatic disruption if $N/N_{\rm max} \gg N_{\rm ce}/N_{\rm max}$, i.e. above the horizontal line.

Coulomb disruption. For times larger than $t_{\rm crit}$, i.e. $t > t_{\rm crit}$, cloud particles of a given size will explode due to the electrostatic force. The solution for $t_{\rm crit}$ is depicted in Fig 6.

3.3 Grain charge deposition time-scales in ultra-cool atmospheres of extrasolar planets

Approach: We evaluate the maximum charge number densities possible through charge adsorption and the critical survival time scale against electrostatic disruption of mineral cloud particles in the ionised gases of extrasolar atmospheres. We utilised one example DRIFT-PHOENIX atmosphere simulation (Witte, Helling & Hauschildt 2009; Witte et al. 2011) and use the model results for the local gas density, $n_{\rm gas}(z)$ [cm^{-3}], the gas temperature, $T_{\rm gas}(z)$ [K] ($\approx$ 0.1eV), and the cloud particle size $a(z)$ [cm] in order to evaluate Eq. 8, and the critical time scale, $t = t_{\rm crit}$, from $N_{\rm e,d} = N_{\rm ce}$ with Eqs.14 & 15. We represent the cloud particle size a by the height-dependent mean particle size, $\langle a(z)\rangle$ instead of a height-dependent particle size distribution function. We demonstrate the results for the model simulation of a giant gas planet atmosphere with the effective temperature $T_{\rm eff}$ = 1600 K (total radiative flux), the surface gravity $\log g$ = 3, and the set of solar element abundances. The electron velocity, $v_e(z)$ [cm/s], is calculated assuming $T_{\rm e}(z) = T_{\rm gas}(z)$ unless stated otherwise. The first-order ionization rate, ζ [s^{-1}] is used as parameter and different values are explored.

Results: We first explore the atmospheric regions in our example giant gas planet/brown dwarf atmosphere where the cloud particles are stable against electrostatic disruption cause by the charges accumulated on their surfaces. This can be accomplished by comparing the number of charges necessary for Coulomb explosion, $N_{\rm ce}$ (Eq. (15), to the maximum possible number of charges that a cloud par-

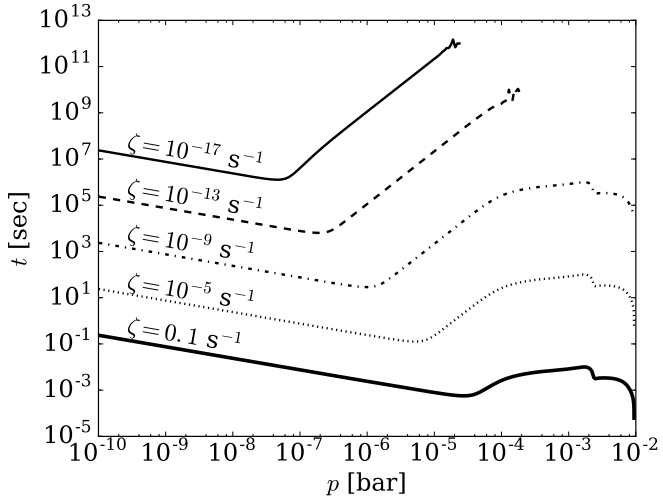

Figure 6. The timescale to coulomb explosion, $t = t_{\rm crit}$ [s], as function of gas pressure, p [dyn/cm^2], for various values of ζ [s^{-1}]. The plots result from applying the parameters of a DRIFT-PHOENIX model atmosphere ($\log g = 3$, $T_{\rm eff} = 1600$). Example values are: Cosmic-ray ionization ionization rate: $\zeta = 10^{-13}$ s^{-1}, extensive air showers: $\zeta \sim 10^{-9}$s^{-1}.

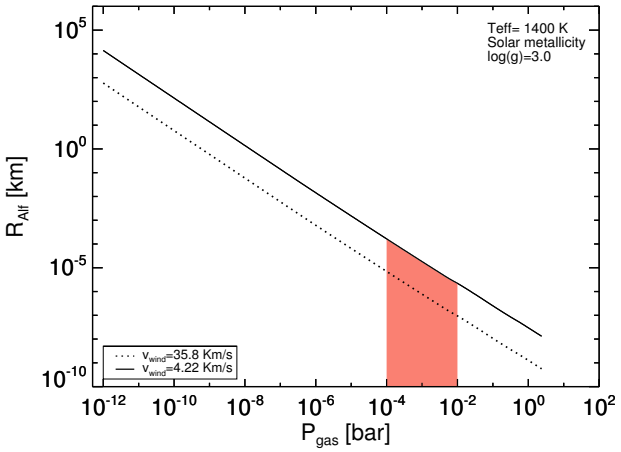

Figure 7. Size of cloud holes, $R_{\rm Alf}(z) = v_{\rm wind}/\nu_{\rm ni}(z)$, that would be caused by Alfvén ionisation induced electrostatic cloud particle destruction if the respective hydrodynamic wind speeds can be reached. $R_{\rm Alf}$ is calculated for two cases: **solid line:** wind speed reached values to ionise hydrogen ($v_{\rm wind} = 38.5$ km s^{-1}, $n_{\rm gas} = n_{<H>}$, $v_{\rm th,i} = v_{\rm th,H^-}$), **dotted line:** wind speed reached values to ionise K ($v_{\rm wind} = 4.22$ km s^{-1}, $n_{\rm gas} = n_{<H>}$, $v_{\rm th,i} = v_{\rm th,K^+}$). The red-shaded area is the pressure range where dynamic atmosphere models reach maximum values of $5 \ldots 6$ km s^{-1}.

ticle can adsorb from the ionised atmosphere, $N_{\rm max}$ (Eq. 8),

$$\frac{N_{\rm ce}}{N_{\rm max}} = \sqrt{\frac{e^2\Sigma_s}{8\epsilon_0}}\frac{\pi\langle a\rangle}{T_e} \qquad (16)$$

where T_e [eV] is the electron temperature. Only if $N_{\rm ce}/N_{\rm max} \gg 1$, the cloud particles are stable against electrostatic disruption for a given electron temperature, $T_{\rm e}$. Coulomb explosion will only take place if $N_{\rm ce}/N_{\rm max} \ll 1$. Figure 5 demonstrates that in the model atmosphere considered here, T_e needs to be much greater than the thermal energy to achieve $N_{\rm ce}/N_{\rm max} \ll 1$. Since the average composition of the dust will change as a function of atmospheric height, this value of Σ_s will vary between 1 MPa and 100 MPa, and we set $\Sigma_s = 50$ MPa for the exploratory purpose of this paper. Generally, the cloud layer is stable against Coulomb explosion for $T_{\rm e} < 10^5$ K (< 10eV) and at high pressures inside the atmosphere also above 10^5K (Fig. 5).

The timescale for Coulomb explosion to occur can be derived from Eq. (14) using setting $N = N_{\rm ce}$ for a given grain size (Eq. 15). This timescale is plotted as a function of atmospheric pressure $p_{\rm gas}$ [dyn/cm^2] in Figure 6, and the ionisation rate parameter is explored. The timescale for Coulomb explosion depends critically upon the ionization rate. For fast electrons, when $T_e > 10$ eV ($\approx 10^5$K) , the timescale ranges from about 100 days for a weak source of ionization, $\zeta = 10^{-17}$ s^{-1}. For cosmic rays as an example of a weak ionisation source, the timescale for Coulomb explosion drops to on the order of one day, and for strong ionizing process, such as Alfvén ionization, the timescale drops significantly to between 1 μs to 1 ms. This broad range of timescales means that the ionizing source has a significant effect on the size distribution of grains in the upper atmosphere. This leads in particular to the conclusion that the occurrence of highly efficient local ionisation processes like Alfvén ionization lead to a local destruction of cloud particles through electrostatic effects. The resulting sputtering products increase the number of small grains which will lead to a local increase of cloud opacity. Each of these sputtering products may carry different charges depending on their individual size. There is no reason to believe that sputtering products are of the same size similar to mechanical destruction processes (e.g. Güttler et al. 2010). Cloudy atmosphere of brown dwarfs with strong winds that result in Alfvén ionization could therefore mimic the presence of star spots or similar variability pattern if the affected area is large enough. The 'dark spot' would only be present until the cloud particles have grown to larger sizes so that no opacity contrast to its surrounding will be detectable any more. The size of such spots would be $R_{\rm Alf} \approx v_{\rm wind}/\nu_{\rm ni}$ assuming the ion can follow the hydrodynamic wind. Figure 7 demonstrate the potential sizes of such spots for the case of a fully ionised molecular hydrogen gas (solid line) and the case of that only potassium (K, dotted line) could be ionised. Simulations by Dobbs-Dixon & Agol (2013) show that a maximum wind speed of $5 \ldots 6$ km s^{-1} is reached in the pressure interval $p_{\rm gas} = 10^{-4} \ldots 10^{-2}$ bar (red shaded area) in an irradiated giant gas planet atmosphere. Similar models for irradiated brown dwarfs are not available yet. Brown dwarf circulation models for non-irradiated but fast rotating objects achieve hydrodynamic velocities in the atmosphere below the necessary Alfvén ionization threshold at present (Zhang & Showman 2014). In the case of a giant gas planets were the local wind speed is sufficient inside the atmosphere where $p_{\rm gas} = 10^{-4} \ldots 10^{-2}$ bar, the diameter of an Alfvén ionization induced cloud hole would be 0.1m at the lowest pressure end of the interval, too small to make any observational effect. If appropriate velocities occur at lower pressures, cloud-free spots could be just 10m of size, still far below an observational effect.

4 SUMMARY

Thermal ionisation in brown dwarf and giant gas planet atmospheres with local temperatures between 100K . . . 4000K and high local gas pressures between 10^{-7}bar . . . 5bar allows for electrostatic interactions and magnetic coupling of such ultra-cool and chemically rich gases. Non-equilibrium processes like cosmic ray ionisation and discharge processes in clouds will increase the local pool of free electrons for a certain time which will, however, not increase the magnetic field coupling which is mainly determined by a rather strong magnetic field density in particular in brown dwarfs. Cosmic rays and lighting discharges do have a distinct effect on the composition of the local atmospheric gas. Cosmic rays affect the atmosphere through air showers which were modelled with a 3D Monte Carlo radiative transfer code to be able to visualise their spacial extent. Only the upper-most atmospheric layers of extrasolar planets and brown dwarfs are effected by cosmic ray triggered air showers similar to solar system planets.

Atmospheres of giant gas planets and brown dwarfs are so cold that clouds made of mixed-material mineral particles that condense directly from the gas phase. Gravitational settling (rain out) determines the vertical extension and causes a large-scale charge separation of charged cloud particles of different sizes. Cloud particles are charged due to triboelectric processes in such highly dynamic atmospheres. This dynamics is driven by irradiation or rotation which links the planet and brown dwarf to its stellar and galactic environment. If hydrodynamic winds achieve high enough local speeds, Alvén ionisation creates pockets of a high degree of ionisation. The free electrons will interact with the cloud particles and electrons will contribute to the charge accumulation on the grain surface. We estimate that this process is too inefficient to cause an electrostatic disruption of the cloud particles, hence, the cloud particles will not be destroyed by Coulomb explosion for the local temperature in the collisional dominated brown dwarf and giant gas planet atmospheres. If, however, the ionisation rate of the atmosphere increases, Coulomb explosion may cause the emergence of cloud holes. The potential size of such holes in an extended cloud deck is too small and would occur to far inside the cloud to mimic the effect of magnetic field induced star spots.

ACKNOWLEDGMENTS

We highlight financial support of the European Community under the FP7 by the ERC starting grant 257431.

REFERENCES

Allard F., 1995, Nature, 378, 441
Bailey R. L., Helling Ch., Hodosán G., Bilger C., Stark C. R., 2014, ApJ, 784, 43
Burrows A. et al., 1997, ApJ, 491, 856
Diver D. A., Fletcher L., Potts H. E., 2005, Sol Phys, 227, 207
Dobbs-Dixon I., Agol E., 2013, MNRAS, 435, 3159
Dobbs-Dixon I., Cumming A., Lin D. N. C., 2010, ApJ, 710, 1395
Dubrovin D., Nijdam S., Clevis T. T. J., Heijmans L. C. J., Ebert U., Yair Y., Price C., 2015, Journal of Physics D Applied Physics, 48, 055205
Dupree S. A., Fraley S. K., 2002, A Monte Carlo Primer
Fortney J. J., Marley M. S., Saumon D., Lodders K., 2008, ApJ, 683, 1104
Fujii Y. I., Okuzumi S., Inutsuka S.-i., 2011, ApJ, 743, 53
Gizis J. E. et al., 2015, ApJ, 813, 104
Gurevich A. V., Karashtin A. N., 2013, Physical Review Letters, 110
Güttler C., Blum J., Zsom A., Ormel C. W., Dullemond C. P., 2010, A&A, 513, A56
Hallinan G. et al., 2015, Nature, 523, 568
Hauschildt P. H., Baron E., 1999, Journal of Computational and Applied Mathematics, 109, 41
Helling Ch., Casewell S., 2014, A&A Review, 22, 80
Helling Ch., Dehn M., Woitke P., Hauschildt P. H., 2008a, ApJL, 675, L105
Helling Ch., Dehn M., Woitke P., Hauschildt P. H., 2008b, ApJL, 677, L157
Helling Ch., Fomins A., 2013, Philosophical Transactions of the Royal Society of London Series A, 371, 10581
Helling Ch., Jardine M., Mokler F., 2011, ApJ, 737, 38
Helling Ch., Jardine M., Stark C., Diver D., 2013, ApJ, 767, 136
Helling Ch., Jardine M., Witte S., Diver D. A., 2011, ApJ, 727, 4
Helling Ch., Woitke P., 2006, A&A, 455, 325
Helling Ch., Woitke P., Thi W.-F., 2008a, A&A, 485, 547
Helling Ch., Woitke P., Thi W.-F., 2008b, A&A, 485, 547
Ilgner M., 2012, A&A, 538, A124
Marley M. S., Ackerman A. S., Cuzzi J. N., Kitzmann D., 2013, Clouds and Hazes in Exoplanet Atmospheres, Mackwell S. J., Simon-Miller A. A., Harder J. W., Bullock M. A., eds., pp. 367–391
Marley M. S., Seager S., Saumon D., Lodders K., Ackerman A. S., Freedman R. S., Fan X., 2002, ApJ, 568, 335
Mohanty S., Basri G., Shu F., Allard F., Chabrier G., 2002, ApJ, 571, 469
Nichols J. D., Burleigh M. R., Casewell S. L., Cowley S. W. H., Wynn G. A., Clarke J. T., West A. A., 2012, ApJ, 760, 59
Rimmer P. B., Helling Ch., 2013, ApJ, 774, 108
Rimmer P. B., Helling Ch., Bilger C., 2014, International Journal of Astrobiology, 13, 173
Rimmer P. B., Stark C. R., Helling Ch., 2014, ApJL, 787, L25
Rodríguez-Barrera M. I., Helling Ch., Stark C. R., Rice A. M., 2015, MNRAS, 454, 3977
Schmidt S. J., Hawley S. L., West A. A., Bochanski J. J., Davenport J. R. A., Ge J., Schneider D. P., 2015, AJ, 149, 158
Showman A. P., Cooper C. S., Fortney J. J., Marley M. S., 2008, ApJ, 682, 559
Showman A. P., Lewis N. K., Fortney J. J., 2015, ApJ, 801, 95
Sorahana S., Suzuki T. K., Yamamura I., 2014, MNRAS, 440, 3675
Stark C. R., Helling Ch., Diver D. A., 2015, A&A, 579, A41
Stark C. R., Helling Ch., Diver D. A., Rimmer P. B., 2013, ApJ, 776, 11
Vorgul I. et al., 2011, Physics of Plasmas, 18, 056501
Williams P. K. G., Casewell S. L., Stark C. R., Littlefair S. P., Helling Ch., Berger E., 2015, ArXiv e-prints
Witte S., Helling Ch., Barman T., Heidrich N., Hauschildt P. H., 2011, A&A, 529, A44
Witte S., Helling Ch., Hauschildt P. H., 2009, A&A, 506, 1367
Woitke P., Helling Ch., 2003, A&A, 399, 297
Woitke P., Helling Ch., 2004, A&A, 414, 335
Wood K., Reynolds R. J., 1999, ApJ, 525, 799
Zhang X., Showman A. P., 2014, ApJL, 788, L6